Evolution and Final Fates of a Rotating 25 $M_\odot$ Pop III Star

Amar ARYAN[1,2,*], Shashi Bhushan PANDEY[1], Rahul GUPTA[1,2], Sugriva Nath TIWARI[2]
and Amit Kumar ROR[1]

[1] Aryabhatta Research Institute of observational sciencES (ARIES), Nainital, Uttarakhand, India-263001

[2] Department of Physics, Deen Dayal Upadhyaya Gorakhpur University, Gorakhpur, Uttar Pradesh, India-273009

* Corresponding author: amararyan941@gmail.com and amar@aries.res.in

Abstract

In this manuscript, we present the one-dimensional stellar evolution of two rotating population III (Pop III) star models, each having a mass of 25 $M_\odot$ at the zero-age main-sequence (ZAMS). The slowly rotating model has an initial angular rotational velocity of 10% of the critical angular rotational velocity. In contrast, the rapidly rotating model has an initial angular rotational velocity of 70% of the critical angular rotational velocity. As an effect of rotationally enhanced mixing, we find that the rapidly rotating model suffers an enormous mass loss due to the deposition of a significant amount of CNO elements toward the surface after the main-sequence phase. We also display the simulated light curves as these models explode into core-collapse supernovae (CCSNe).

Keywords: Population III stars, Stellar evolution, Hydrodynamic simulation, Supernovae

1. Introduction

Population III stars refer to the first generation of stars, a captivating and enigmatic class of astrophysical objects that were thought to be born in the early Universe before the formation of any other stars. These primordial stars are believed to have formed from initial, pristine gas composed almost entirely of hydrogen and helium, lacking any heavier elements (Bond, 1981; Cayrel, 1986). Because of their unique composition and lack of any coolant in the early Universe, Pop III stars are thought to have been much more massive than stars in the later generations (Hirano et al., 2015). They played a crucial role in shaping the Universe as their intense radiation ionized the surrounding gas to initiate the process of cosmic reionization (Bromm, 2013). While no Population III stars have been directly observed yet, their existence is supported by theoretical models (e.g., among many others Nakamura and Umemura, 1999; O'Shea and Norman, 2007) and indirect evidence (e.g., among many others Chen et al., 2014; Visbal et al., 2015; Ricotti, 2016; Matsumoto et al., 2016; Mirocha et al., 2018). The studies related

to these first-ever stellar objects are the key to unveil the mysteries of the early Universe and are also very important to understand the origins of other Pop II and Pop I stars. There are multiple studies to understand the possible existence, evolution, and final fates of Pop III stars (e.g., among many others, Marigo et al., 2003; Ekström et al., 2008; Turk et al., 2009; Yoon et al., 2012; Hirano et al., 2014; Ishiyama et al., 2016; Windhorst et al., 2018; Murphy et al., 2021; Aryan et al., 2023). In this work, we investigate the cause of enormous mass loss in rapidly rotating model as it passes through various stages of its evolution. We also present the hydrodynamic simulations of synthetic explosions of the models at the onset of core collapse.

We have divided this manuscript into four sections. We present a brief overview of the literature in Sect. 1. The numerical settings of the models to perform their stellar evolution are presented in Sect. 2 while the methods to simulate the synthetic explosions are discussed in Sect. 3. Finally, we present our results and conclusions in Sect. 4.

2. Evolution of the Models up to Pre-SN stage

To perform the stellar evolution of the models, we utilise the modules for experiments in stellar astrophysics (MESA) with version number mesa-r21.12.1 (Paxton et al., 2011, 2013, 2015, 2018). Here we take two $25\,M_\odot$ ZAMS star models with zero metallicity and perform their one-dimensional stellar evolution until they reach the onset of the core-collapse phase. The models are marked to have reached the onset of the core-collapse stage if any location within the star model hits an infall velocity of $500\,\mathrm{km\,s^{-1}}$. The MESA settings for the calculations presented here are similar to the ones used in Aryan et al. (2021a, 2022a,b) and closely follow Aryan et al. (2023). However, we list a few critical changes. We have performed the stellar evolution of two models with initial rotations ($\Omega/\Omega_{\mathrm{crit}}$) of 0.1 and 0.7, respectively. In this work, we have also investigated the effect of changing the wind scaling factor (η) from 0.5 to 1.0. The models presented in this work are named so that they contain information on initial ZMAS mass, metallicity, scaling factor, and rotation. The slowly rotating model named M25_Z0.00_η1.0_Rot0.1 refers to a star with a ZAMS mass of $25\,M_\odot$, zero metallicity, $\eta = 1.0$, and an initial rotation of 0.1. Similarly, the rapidly rotating model named M25_Z0.00_η1.0_Rot0.7 refers to a star with a ZAMS mass of $25\,M_\odot$, zero metallicity, $\eta = 1.0$, and an initial rotation of 0.7. The left-hand panel of Fig. 1 shows the variation of the core-temperature (T_{core}) vs. core-density (ρ_{core}) curve as the models evolve from the ZAMS to core-collapse phase. The Pre-SN parameters are mentioned in Table 1. The right-hand panel of Fig. 1 shows the Pre-SN radii of the two models. The rapidly rotating model has undergone significant mass loss, resulting in a very small Pre-SN radius. In contrast, the slowly rotating model has retained most of its outer hydrogen-envelope. Another effect evident as a result of increasing η from 0.5 to 1.0 is an increased loss of mass in the rapidly rotating model considered here. Although the M25_Z0.00_Rot0.8 model from Aryan et al. (2023) has a greater initial rotation than the M25_Z0.00_η1.0_Rot0.7 model here, the latter looses much more mass than the previous one due to an increased η. Additionally, we have found that the rapidly rotating model suffered an enormous mass loss compared to the slowly rotating model. We have performed a diagnosis to explain this enormous mass loss. The four panels of Fig. 2 display the mass fractions of several elements after the main-sequence
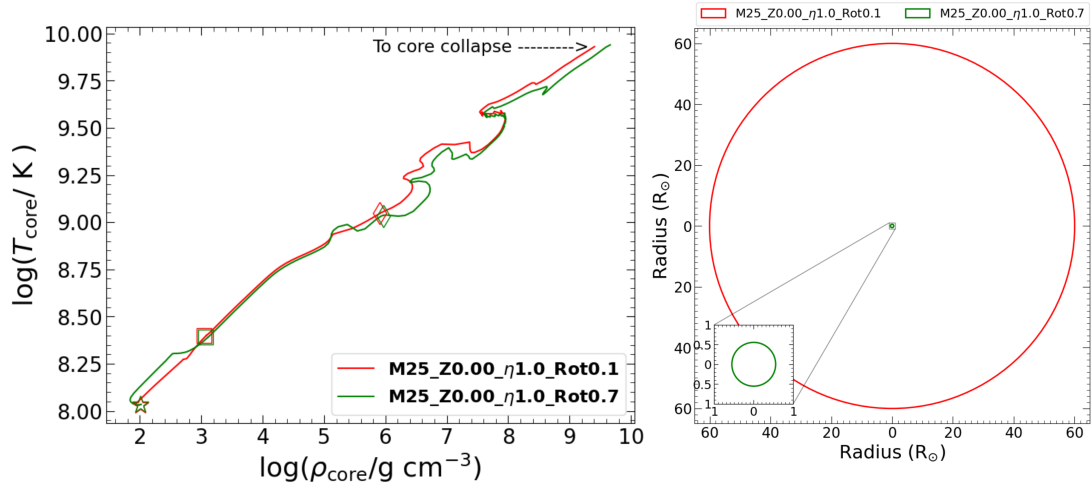
Figure 1: (*Left*) Evolution of the T_{core} vs. ρ_{core} as our Pop III models evolve on the HR diagram. The phases of arrival on ZAMS, the exhaustion of core–He burning, and the exhaustion of core-C burning are indicated by hollow stars, squares, and diamonds, respectively. (*Right*) Pre-SN radii of the models. The rapidly rotating model seems to have suffered enormous mass loss and thus possesses a very small Pre-SN radius.

Table 1: (*Top*) The Pre-SN properties of the two models using `MESA`, where M_{Pre-SN} is the mass at the Pre-SN stage, T_{eff} the effective temperature, R_{Pre-SN} the radius at the Pre-SN stage, and $\log_{10} L_{Pre-SN}/L_{\odot})$ the luminosity at the Pre-SN stage. (*Bottom*) The corresponding `SNEC` explosion parameters, where M_c is the excised central remnant mass, M_{ej} the ejecta mass, V_{boost} the boosting-velocity of the first two computational cells in the model profile, and E_{exp} the explosion energy.

	Pre-SN			
Model Name	M_{Pre-SN}	T_{eff}	R_{Pre-SN}	$\log_{10}(L_{Pre-SN}/L_{\odot})$
	$(M_{\odot})$	(K)	$(R_{\odot})$	
M25_Z0.00_η1.0_Rot0.1	24.99	16172	60.04	5.345
M25_Z0.00_η1.0_Rot0.7	7.71	167875	0.55	5.340

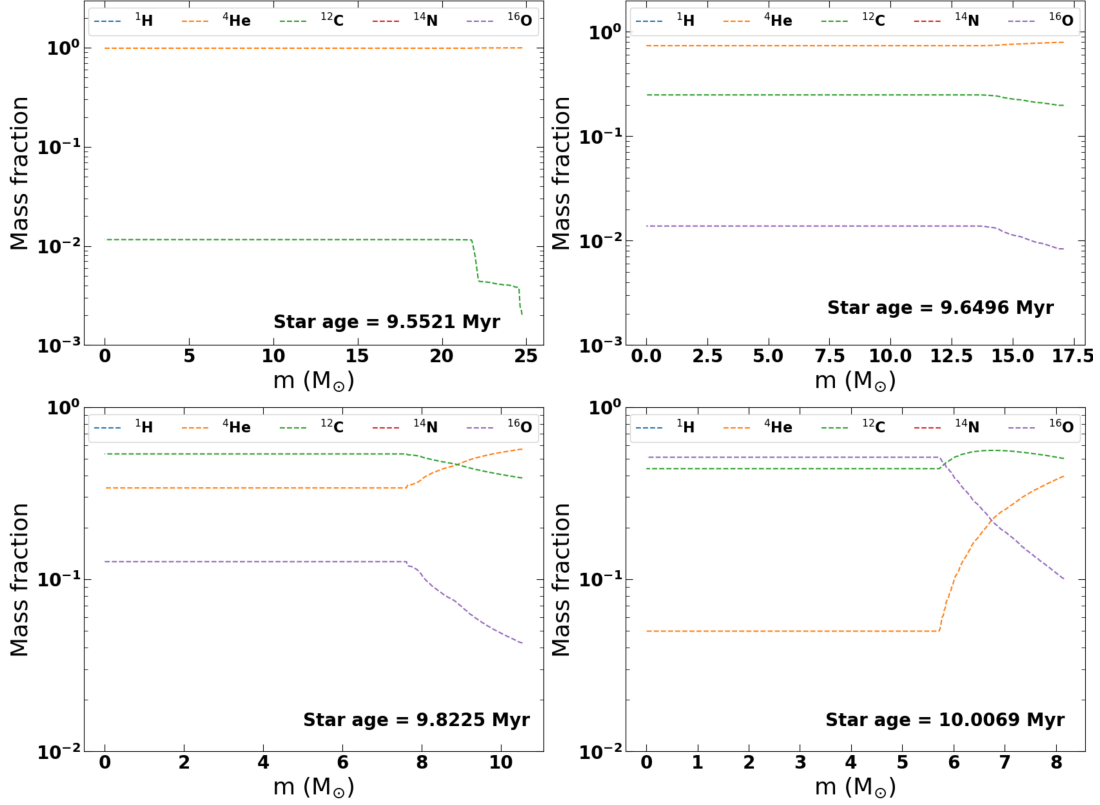|	*Explosion*			
Model Name	M_c	M_{ej}	V_{boost}	E_{exp}
	$(M_{\odot})$	$(M_{\odot})$	$(10^9 \, cm \, s^{-1})$	$(10^{51} \, erg)$
M25_Z0.00_η1.0_Rot0.1	1.60	23.39	4.0	6.58
M25_Z0.00_η1.0_Rot0.7	1.50	6.21	4.0	4.07

Figure 2: This set of four figures shows the mass fraction of the rapidly rotating model (M25_Z0.00_η1.0_Rot0.7) at four epochs after the main-sequence phase. The increased fractions of CNO elements near the surface dramatically boost the surface metallicity.

phase. As the model progresses on the HR diagram beyond the main-sequence, the fractions of CNO elements toward the surface increase, dramatically enhancing surface metallicity. The increased surface metallicity, in turn, enhances mass loss (Hirschi, 2007).

3. Explosion of the Pre-SN Models

Once the models reach the core-collapse stage, we simulate their synthetic explosions utilising SNEC (Morozova et al., 2015). Most of the SNEC settings are similar to those in Ouchi and Maeda (2019); Aryan et al. (2021b, 2022c, 2023). Here, we mention important modifications. We choose the "Piston_Explosion" option to simulate the synthetic explosion with a set of 700 grid cells using SNEC. For CCSNe, the "Piston_Explosion" might be the more realistic one since these SNe are thought to be arising due to the shock wave bouncing back from the neutron star. On the other hand, the "Thermal_Bomb" type is better suited for thermonuclear explosions, like Type Ia SNe. As we utilise the "Piston_Explosion" in SNEC, the first two computational cells in our model's profile are subjected to an outward velocity boost (in cm s^{-1}) provided by the "piston_vel" control. We choose "piston_vel = 4d9" for both models. The period of velocity boost lasts for 0.01 s.

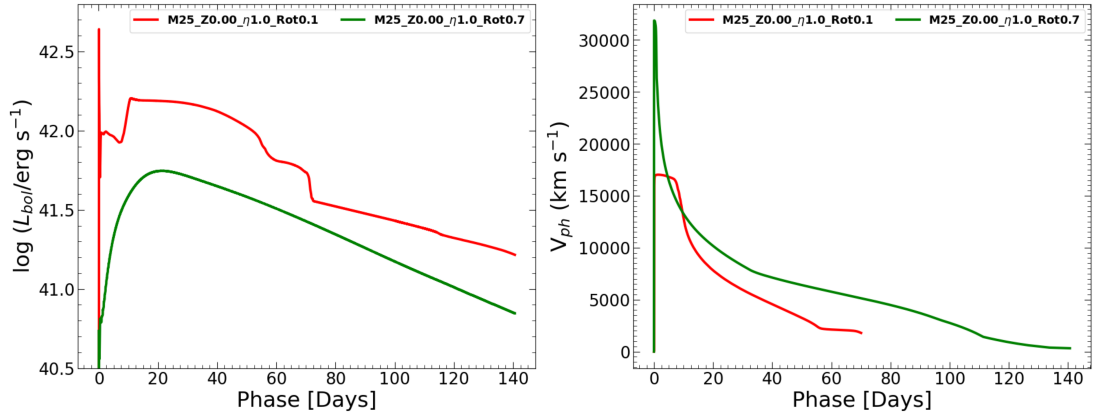For each model considered in this work, we first excise the mass of the final remnant (M_c),

Figure 3: (*Left*) Bolometric luminosity light curves of the two models considered in this work, resulting from the hydrodynamic simulations of their synthetic explosions utilising SNEC. (*Right*) Evolution of corresponding photospheric velocities obtained from SNEC.

which is nearly the mass of the inert iron-core. Additionally, we use an amount of $0.05\,M_\odot$ of ^{56}Ni synthesised for both the models. This quantity of synthesised ^{56}Ni is distributed between the excised central remnant mass cut and the preferred mass coordinate, which is in close proximity to the outer surface of the models. The difference between the Pre-SN mass, $M_{\mathrm{Pre-SN}}$, and M_{c} is the corresponding ejecta mass for each model. We present the detailed explosion parameters in Table 1. The left-hand panel of Fig. 3 shows the bolometric luminosity light curves for the two models. The slowly rotating model has retained most of its outer hydrogen-envelope; thus, its explosion results in a hydrogen-rich SN. The bolometric light curve closely resembles the Type IIP SNe light curves. In contrast, the rapidly rotating model has suffered extensive mass loss. Thus, it explodes as a hydrogen-stripped SN. The bolometric light curve from the rapidly rotating model mimics the light curves of hydrogen-deficient Type Ib/c SNe. The right-hand panel of Fig. 3 displays the corresponding photospheric velocity evolution for the two models. The slowly rotating model resembles the photospheric velocities shown by Type IIP SNe, while the very high initial photospheric velocities resemble stripped-envelope SNe.

4. Results and Conclusions

In this manuscript, we modelled the one-dimensional stellar evolution of two rotating Pop III models until they reached the stage of the onset of core collapse utilising MESA. Further, we also performed the hydrodynamic simulations of their synthetic explosions using the models at the onset of core collapse in appropriate form as input to SNEC. Our main findings are as follows:

1. We explicitly explored the cause of extensive mass loss in our rapidly rotating model by investigating the mass fraction plots at different stages after the main-sequence phase. We find that the increase in mass loss rates can be attributed to the dramatic increase in surface metallicity.

2. We found that increasing η from 0.5 to 1.0 also played an essential role in increasing the mass loss.

3. Unlike Aryan et al. (2023), in this work, we simulated the piston-driven explosion. However, we hardly see much difference in our results.

Acknowledgments

Further Information

Authors' ORCID identifiers

0000-0002-9928-0369 (Amar ARYAN)
0000-0002-1474-1980 (Shashi Bhushan PANDEY)
0000-0003-4905-7801 (Rahul GUPTA)
0000-0003-3164-8056 (Amit Kumar ROR)

Author contributions

This work is part of a collective effort with contributions from all the co-authors.

Conflicts of interest

The authors declare no conflict of interest.

References

Aryan, A., Pandey, S. B., Gupta, R. and Ror, A. K. (2023) Evolution of rotating $25\,M_\odot$ Population III star: physical properties and resulting supernovae. MNRAS, 521(1), L17–L23. https://doi.org/10.1093/mnrasl/slad020.

Aryan, A., Pandey, S. B., Kumar, A., Gupta, R., Castro-Tirado, A. J. and Tiwari, S. N. (2021a) Study of energetic transients using tools like MESA & SNEC, MOSFiT and SNCOSMO. In VI Workshop on Robotic Autonomous Observatories, edited by Castro-Tirado, A. J., Pandey, S. B. and Caballero-García, M. D., vol. 53 of *RMxAC*, pp. 215–224. https://doi.org/10.22201/ia.14052059p.2021.53.41.

Aryan, A., Pandey, S. B., Kumar, A., Gupta, R., Ror, A. K., Tripathi, A. and Tiwari, S. N. (2022a) Analyses of hydrogen-stripped core-collapse supernovae using MOSFiT and MESA-based tools. JApA, 43(2), 87. https://doi.org/10.1007/s12036-022-09866-z.

Aryan, A., Pandey, S. B., Yadav, A. P., Gupta, R. and Tiwari, S. N. (2022b) Core-collapse supernova from a possible progenitor star of $100\,M_\odot$. JApA, 43(1), 2. https://doi.org/10.1007/s12036-021-09784-6.

Aryan, A., Pandey, S. B., Zheng, W., Filippenko, A. V., Vinko, J., Ouchi, R., Brink, T. G., Halle, A., Molloy, J., Kumar, S., Halevi, G., Kilpatrick, C. D., Kumar, A., Gupta, R. and Ror, A. K. (2022c) SN 2016iyc: a type IIb supernova arising from a low-mass progenitor. MNRAS, 517(2), 1750–1766. https://doi.org/10.1093/mnras/stac2326.

Aryan, A., Pandey, S. B., Zheng, W., Filippenko, A. V., Vinko, J., Ouchi, R., Shivvers, I., Yuk, H., Kumar, S., Stegman, S., Halevi, G., Ross, T. W., Gould, C., Yunus, S., Baer-Way, R., deGraw, A., Maeda, K., Bhattacharya, D., Kumar, A., Gupta, R., Yadav, A. P., Buckley, D. A. H., Misra, K. and Tiwari, S. N. (2021b) Progenitor mass constraints for the type Ib intermediate-luminosity SN 2015ap and the highly extinguished SN 2016bau. MNRAS, 505(2), 2530–2547. https://doi.org/10.1093/mnras/stab1379.

Bond, H. E. (1981) Where is Population III? ApJ, 248, 606–611. https://doi.org/10.1086/159186.

Bromm, V. (2013) Formation of the first star. RPPh, 76(11), 112901. https://doi.org/10.1088/0034-4885/76/11/112901.

Cayrel, R. (1986) And if Population III were Population II? A&A, 168, 81–88.

Chen, K.-J., Heger, A., Woosley, S., Almgren, A. and Whalen, D. J. (2014) Pair instability supernovae of very massive Population III stars. ApJ, 792(1), 44. https://doi.org/10.1088/0004-637X/792/1/44.

Ekström, S., Meynet, G., Chiappini, C., Hirschi, R. and Maeder, A. (2008) Effects of rotation on the evolution of primordial stars. A&A, 489(2), 685–698. https://doi.org/10.1051/0004-6361:200809633.

Hirano, S., Hosokawa, T., Yoshida, N., Omukai, K. and Yorke, H. W. (2015) Primordial star formation under the influence of far ultraviolet radiation: 1540 cosmological haloes and the stellar mass distribution. MNRAS, 448(1), 568–587. https://doi.org/10.1093/mnras/stv044.

Hirano, S., Hosokawa, T., Yoshida, N., Umeda, H., Omukai, K., Chiaki, G. and Yorke, H. W. (2014) One hundred first stars: Protostellar evolution and the final masses. ApJ, 781(2), 60. https://doi.org/10.1088/0004-637X/781/2/60.

Hirschi, R. (2007) Very low-metallicity massive stars: Pre-SN evolution models and primary nitrogen production. A&A, 461(2), 571–583. https://doi.org/10.1051/0004-6361:20065356.

Ishiyama, T., Sudo, K., Yokoi, S., Hasegawa, K., Tominaga, N. and Susa, H. (2016) Where are the low-mass Population III stars? ApJ, 826(1), 9. https://doi.org/10.3847/0004-637X/826/1/9.

Marigo, P., Chiosi, C. and Kudritzki, R. P. (2003) Zero-metallicity stars. II. Evolution of very massive objects with mass loss. A&A, 399, 617–630. https://doi.org/10.1051/0004-6361:20021756.

Matsumoto, T., Nakauchi, D., Ioka, K. and Nakamura, T. (2016) The jet-powered supernovae of $\sim 10^5 M_\odot$ Population III stars are observable by *Euclid*, *WFIRST*, *WISH*, and *JWST*. ApJ, 823(2), 83. https://doi.org/10.3847/0004-637X/823/2/83.

Mirocha, J., Mebane, R. H., Furlanetto, S. R., Singal, K. and Trinh, D. (2018) Unique signatures of Population III stars in the global 21-cm signal. MNRAS, 478(4), 5591–5606. https://doi.org/10.1093/mnras/sty1388.

Morozova, V., Piro, A. L., Renzo, M., Ott, C. D., Clausen, D., Couch, S. M., Ellis, J. and Roberts, L. F. (2015) Light curves of core-collapse supernovae with substantial mass loss using the new open-source SuperNova Explosion Code (SNEC). ApJ, 814(1), 63. https://doi.org/10.1088/0004-637X/814/1/63.

Murphy, L. J., Groh, J. H., Ekström, S., Meynet, G., Pezzotti, C., Georgy, C., Choplin, A., Eggenberger, P., Farrell, E., Haemmerlé, L., Hirschi, R., Maeder, A. and Martinet, S. (2021) Grids of stellar models with rotation – V. Models from 1.7 to $120\,M_\odot$ at zero metallicity. MNRAS, 501(2), 2745–2763. https://doi.org/10.1093/mnras/staa3803.

Nakamura, F. and Umemura, M. (1999) On the mass of Population III stars. ApJ, 515(1), 239–248. https://doi.org/10.1086/307020.

O'Shea, B. W. and Norman, M. L. (2007) Population III star formation in a ΛCDM universe. I. The effect of formation redshift and environment on protostellar accretion rate. ApJ, 654(1), 66–92. https://doi.org/10.1086/509250.

Ouchi, R. and Maeda, K. (2019) Constraining massive star activities in the final years through properties of supernovae and their progenitors. ApJ, 877(2), 92. https://doi.org/10.3847/1538-4357/ab1a37.

Paxton, B., Bildsten, L., Dotter, A., Herwig, F., Lesaffre, P. and Timmes, F. (2011) Modules for Experiments in Stellar Astrophysics (MESA). ApJS, 192(1), 3. https://doi.org/10.1088/0067-0049/192/1/3.

Paxton, B., Cantiello, M., Arras, P., Bildsten, L., Brown, E. F., Dotter, A., Mankovich, C., Montgomery, M. H., Stello, D., Timmes, F. X. and Townsend, R. (2013) Modules for Experiments in Stellar Astrophysics (MESA): Planets, oscillations, rotation, and massive stars. ApJS, 208(1), 4. https://doi.org/10.1088/0067-0049/208/1/4.

Paxton, B., Marchant, P., Schwab, J., Bauer, E. B., Bildsten, L., Cantiello, M., Dessart, L., Farmer, R., Hu, H., Langer, N., Townsend, R. H. D., Townsley, D. M. and Timmes, F. X. (2015) Modules for Experiments in Stellar Astrophysics (MESA): Binaries, pulsations, and explosions. ApJS, 220(1), 15. https://doi.org/10.1088/0067-0049/220/1/15.

Paxton, B., Schwab, J., Bauer, E. B., Bildsten, L., Blinnikov, S., Duffell, P., Farmer, R., Goldberg, J. A., Marchant, P., Sorokina, E., Thoul, A., Townsend, R. H. D. and Timmes, F. X. (2018) Modules for Experiments in Stellar Astrophysics (MESA): Convective boundaries, element diffusion, and massive star explosions. ApJS, 234(2), 34. https://doi.org/10.3847/1538-4365/aaa5a8.

Ricotti, M. (2016) X-ray twinkles and Population III stars. MNRAS, 462(1), 601–609. https://doi.org/10.1093/mnras/stw1672.

Turk, M. J., Abel, T. and O'Shea, B. (2009) The formation of Population III binaries from cosmological initial conditions. Sci, 325, 601–605. https://doi.org/10.1126/science.1173540.

Visbal, E., Haiman, Z. and Bryan, G. L. (2015) Looking for Population III stars with he ii line intensity mapping. MNRAS, 450(3), 2506–2513. https://doi.org/10.1093/mnras/stv785.

Windhorst, R. A., Timmes, F. X., Wyithe, J. S. B., Alpaslan, M., Andrews, S. K., Coe, D., Diego, J. M., Dijkstra, M., Driver, S. P., Kelly, P. L. and Kim, D. (2018) On the observability of individual Population III stars and their stellar-mass black hole accretion disks through cluster caustic transits. ApJS, 234(2), 41. https://doi.org/10.3847/1538-4365/aaa760.

Yoon, S. C., Dierks, A. and Langer, N. (2012) Evolution of massive Population III stars with rotation and magnetic fields. A&A, 542, A113. https://doi.org/10.1051/0004-6361/201117769.